Silicon Corrosion in Neutral Media: The Influence of Confined Geometries and Crevice Corrosion in Simulated Physiological Solutions

Emilija Ilic, [1,2,z] Ainhoa Pardo,[1] Roland Hauert,[1] Patrik Schmutz,[1,*] and Stefano Mischler[2,*]

[1]*Empa, Swiss Federal Laboratories for Materials Science and Technology, Laboratory for Joining Technologies and Corrosion, Switzerland*
[2]*EPFL, Ecole Polytechnique Fédérale de Lausanne, Tribology and Interfacial Chemistry Group, Lausanne, Switzerland*

Silicon (Si) based implantable components are widely used to restore functionalities in the human body. However, there have been reported instances of Si corroding after only a few years of implantation. A key parameter often overlooked when assessing Si stability in-vitro, is the added constricting geometries introduced through in-vivo implantation. The influence of crevices and confined solutions on the stability of Si is presented in this study, considering two simulated physiological solutions: 0.01 M phosphate buffered saline (PBS) and HyClone Wear Test Fluid (WTF). It was found that Si is highly vulnerable to corrosion in confined/crevice conditions. High pitting corrosion susceptibility is found in a crevice, whereas a dissolution rate of ca. 3.6 nm/h at body temperature occurred due to local alkalization within a confined cathodic area. The corrosion rates could be increased by elevating the temperature and yielded linear Arrhenius relations, with activation energies of 106 KJ/mol in 0.01 M PBS and 109 KJ/mol in HyClone WTF, corresponding to a phosphorous-silicon interaction mechanism. Phosphorous species favored corrosion and contributed to enhanced Si dissolution, while chlorides were not so influential, and applied anodic potential induced pseudo-passivation. These results highlight the importance geometrical configurations can have on a material's surface stability.

Silicon (Si) is normally considered as bioinert and therefore envisaged in a series of new applications. For example, Si based microelectronic devices provide new opportunities for the fabrication of neuroprosthetics such as cochlear, retina and spinal implants, for treating neurological deficits.[1,2] Further, due to its good adhesive properties, Si can be used as an interlayer material in coated orthopedic implants such as hip and knee replacements.[3,4] As with most implantable devices however, problems arise when trying to simulate the long-term in-vivo environment during in-vitro testing. There are hence reported instances of Si-based implants corroding in the body or in animal hosts, despite successful in-vitro testing.[5] For example, Diamond-like Carbon (DLC) coated Ti_6Al_4V femoral heads, containing a Si adhesion promoting interlayer, were expected to increase the lifetime of hip implants. In reality, many failed after only a few years of implantation.[6] Focused ion beam (FIB) cuts into the failed hip explants revealed that the Si adhesion promoting interlayer (original thickness of ca. 70–100 nm) had almost completely dissolved at some areas, as shown in Fig. 1. This corrosion phenomenon resulted in severe local delamination of the coating.[7,8] Similarly, a DLC coated CoCrMo toe joint containing a Si interlayer was explanted after 4 years in a patient, due to failure of the interlayer.[9] Platinum (Pt) coated Si microelectrode arrays, for neuroprosthetic applications, showed delamination of the Pt and signs of pitting corrosion on the underlying Si after 994 days in-vivo.[10] Severe corrosion of Si retinal chips was observed after 6 months of implantation in a rabbit, even though no significant damage occurred during in-vitro testing with immersion in phosphate buffered saline (PBS) solution for up to 21 months.[11] Similarly, large dissolution rates of up to 18 μm/year (ca. 2 nm/h) were recorded on polished Si pieces after one year of implantation in an animal host.[12] In some instances, protective coatings were used on Si substrates to suppress corrosion, but they turned out to be ineffective. For example, Si carbide (SiC) and DLC coatings showed poor protection of the underlying Si in saline solutions.[13] The in-vivo environment further promoted dissolution of Si oxide and Si nitride/oxynitride films, leaving the substrate exposed.[14,15]

From a thermodynamic perspective (Pourbaix diagram[16]), Si is stable in the acidic to weakly alkaline domain, due to the formation of a protective Si dioxide (SiO_2) film, ca. 1 nm in thickness, on its surface. Si is mainly known to be unstable in very alkaline solutions (ca. pH>10) due to complexation with hydroxides (OH^-), and in the presence of fluoride (F^-). For these reasons, in micromachining application, Si is mostly etched in strongly alkaline media or hydrofluoric acid-based solutions. In physiological solutions (ca. pH 7.4), Si is expected to passivate (formation of a nm-thick oxide layer), given the electrolyte/surface potential is kept in the stability regime of SiO_2, approximately above −0.8 V_{SHE}. These stability conditions are extrapolated from the standard Si-H_2O system at 25°C and do not account for the presence of specific body ions, proteins, and body temperature (37°C).

A key parameter often overlooked when assessing Si stability in-vitro, is the added geometrical constraints generated through in-vivo implantation. A Si component wedged between body tissues will behave differently than a wafer piece immersed in bulk physiological simulating solution, hence the two conditions cannot accurately be compared. In-vivo, a degradation induced local pH change may occur in areas confined by surrounding body tissue, as a result of pitting and crevice corrosion attack of the implanted material. A similar statement can be made for Si as an interlayer; the thin interlayer is confined between the coating and substrate, and miniature defects in the coating can allow surrounding body fluid to contact the interlayer, forming an electrochemical crevice cell. In addition, electrochemical galvanic coupling can occur between the substrate and interlayer. Hence, it is important to assess the susceptibility of Si to pitting and aggravated crevice corrosion, before real implantable devices are used in-vivo.

In the present study, a thorough investigation of the corrosion behavior of Si in crevices and confined geometrical environments is presented, using a model geometry and electrochemical cells to analyze the different key parameters (temperature, ionic species, pH evolution, applied potential, material conductivity/doping) controlling the degradation mechanisms. Initiation and dissolution kinetics have been assessed by a combination of long-term and temperature accelerated immersion tests in physiological simulating solutions, along with complementary electrochemical and pH measurements. The findings presented can provide insight into the degradation mechanisms responsible for the failure of Si in the body, whether as it relates to coating adhesion interlayers (as described in Fig. 1) or electronic sensors. With this, better predictions of the lifetime and durability of implantable components and Si-based interlayers can be made, and

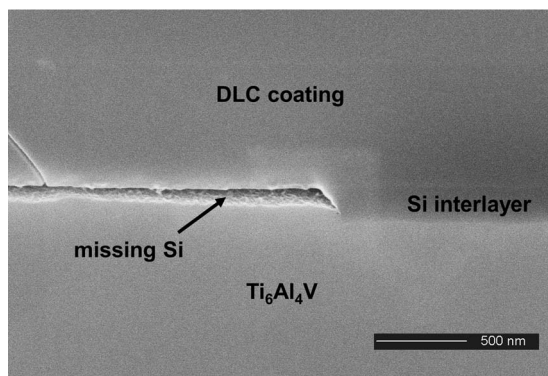*Electrochemical Society Member.
zE-mail: emilija.ilic@empa.ch

Figure 1. FIB cross section of an explanted DLC coated Ti_6Al_4V hip joint ball. Crevice corrosion related attack appears where a Si interlayer has uniformly dissolved away (described further by Hauert et al.[5,6]).

the presented methodologies can as well be applied to any material surface degradation process.

Experimental

Samples and solutions.—Boron (B) doped polished Si (p-type, 1–30 Ω·cm) wafer pieces with a thickness of ca. 0.5 mm and with a (100) crystal orientation, were cleaned by ultrasonic bath in ethanol and dried under argon flow. Corrosion experiments were performed in two different physiological simulating solutions: 0.01 M phosphate buffered saline (PBS, Sigma Aldrich) of pH 7.4, and HyClone Wear Testing Fluid (HyClone WTF, Thermo-Scientific) of pH 7.4–7.7. PBS has a relatively simple formulation, containing 0.137 M NaCl, 0.0027 M KCl, 0.01 M Na_2HPO_4 and 0.0018 M KH_2PO_4. HyClone WTF is bovine serum-based and is designed to simulate human synovial fluid by containing all the relevant body ions (phosphate, chloride, etc.) and 30 g/L of proteins.

Immersion experiments.—Long-term crevice and bulk solution immersion experiments were performed in 0.01 M PBS and HyClone WTF. Using a polyoxymethylene (POM) clamping device, two Si wafer pieces (10 × 10 mm and 20 × 20 mm dimensions) were clamped together (as sketched in Fig. 3a in the initial situation) to form a simple confined/crevice cell (denoted Si│Si) and immersed in 100 mL of 0.01 M PBS or HyClone WTF. Throughout the paper, the term *crevice* will be used to describe the tight space between two clamped counterparts (maximum a few microns in thickness), while the term *confinement* will be used to describe a slightly larger separation (ca. 0.5 mm), directly outside of the crevice or set by a spacer, as described in Fig. 3a. A droplet of the respective solution was placed between the wafer pieces before clamping to ensure the presence of electrolyte inside the crevice area. In order to compare the degradation mechanisms with the situation in bulk solution, single Si wafer pieces were also immersed in 100 mL of each solution. After 35 days of immersion at room temperature (20°C) or 37°C, the samples were unclamped, ultrasonically cleaned in ultrapure water, and dried under argon for further ex-situ surface characterization.

Accelerated immersion experiments were also performed by elevating the temperature and reducing the immersion time accordingly. In 0.01 M PBS, this was done at 50°C, 70°C and 90°C, for 240 h, 24 h, and 5 h, respectively. In HyClone WTF, the experiments were only performed until 50°C in order to avoid substantial protein denaturation.

Electrochemical experiments.—To obtain more detailed information about the Si destabilization mechanisms (initiation, active dissolution), in-situ characterization was implemented. Open circuit potential (OCP) and electrochemical polarization measurements (potentiodynamic and potentiostatic) were conducted on Si

in bulk 0.01 M PBS and HyClone WTF, with a PGSTAT30 potentiostat (Metrohm-Autolab). A three electrodes electrochemical cell setup was used with an exposed Si working electrode (WE) area of 78 mm^2 and an electrolyte volume of 100 mL. A glass Luggin capillary was used as an electrolyte bridge with a 3 M silver/silver chloride (Ag/AgCl) reference electrode (RE, Metrohm). For the electrochemical polarization experiments, a platinum counter electrode (CE, Metrohm) was included and a scan rate of 1 mV/s was applied.

For electrochemical characterization in small electrolyte volumes, a modification of the confined/crevice cell was designed to monitor the OCP of the Si surface at different locations in the confined area, as described in Fig. 2a. Two epoxy blocks with 4 POM screws were used as a clamping device and a 20 × 20 mm Si piece, acting as a WE, was contacted with a copper wire and imbedded into the bottom epoxy block. A 0.5 mm thick polypropylene (PP) spacer with a 10 × 15 mm central cut-out area was placed between the epoxy blocks before clamping, so that a small amount of electrolyte could access the confined area. A 3 M Ag/AgCl RE with an attached salt bridge (a plastic pipette tip filled with agar infused with 1 M NaCl) was inserted through a small hole (Ø = 1 mm) in the top block. A second RE-salt bridge assembly was placed outside of the cell at the confinement opening. With this RE configuration, the OCP could be monitored simultaneously inside and outside of the confined cell, using a multichannel zero-resistance ammeter (ZRA GalvoGill 12, ACM Instruments). The cell with electrodes was immersed in 100 mL of 0.01 M PBS or HyClone WTF, contained within a double-walled glass vessel so that the temperature could be controlled.

Separate measurements were performed at 50°C, followed by 70°C in 0.01 M PBS, and at 37°C, followed by 50°C in HyClone WTF, for 48 h at each temperature. The Si working electrodes were ground with 1000 Grit CarbiMet paper prior to cleaning in order to establish good electrical contact.

In order to determine the pH inside of the confined/crevice cell configuration, the clamping device was slightly modified; a hole was drilled in the opposing epoxy clamp and filled with agar gel infiltrated with a pH indicator, as seen in Fig. 2b. Duplicate immersion experiments were performed with different pH indicators; one with phenolphthalein which turns pink above pH 8.5, and the other with thymolphthalein which turns blue above pH 10.

Post immersion characterization.—After immersion and cleaning treatment, the surfaces of the Si samples were inspected with a scanning electron microscope (SEM, Hitachi S-3700N). In order to quantify the magnitude of corrosive attack, surface profiles were taken over the wafer pieces with a DektakXT stylus profiler (Bruker). The corroded vertical depth was determined by performing several line scans over each sample's surface, measuring the height of the step (Δh) at the crevice/confinement boundary and taking an average value, denoted Δh_{corr}. The corrosion rate could be determined by dividing Δh_{corr} by the immersion time.

Results and Discussion

Long-term immersion experiments in physiological simulating conditions.—The results of the long-term confined/crevice and bulk solution immersion experiments at 37°C exposure in physiological simulating solution are presented before different stress parameters (temperature, ionic concentration) are varied to establish a model for the active corrosion mechanism.

A schematic description of the initial (upon immersion) and resulting (after 35 days) situation of a Si│Si confined/crevice cell immersed in HyClone WTF at 37°C is shown in Fig. 3a. After opening the crevice and cleaning the clamped counterparts, a SEM image was taken of the 20 × 20 mm Si wafer piece over the area containing the crevice mouth (indicated by "0"), as shown in Fig. 3b. Two distinct regions can be seen in the SEM image; one with severe pitting in the crevice area on the left (indicated by "−" arrow), and another uniformly corroded
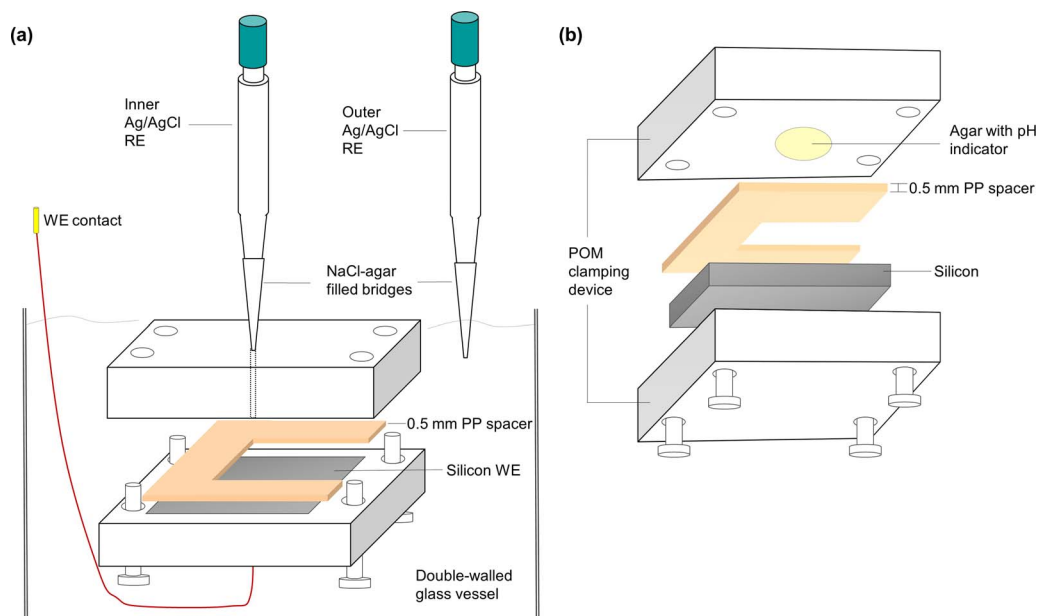
Figure 2. Schematic description of the confinement cell setup (referred as confined/crevice setup in the paper). (a) Used for conducting electrochemical measurements. (b) Modified cell used to determine pH evolution inside a crevice: agar is infiltrated with phenolphthalein (turns pink at pH 8.5–10), or thymolphthalein (turns blue above pH 10) pH indicator, and imbedded in the top clamp.

area in the confinement on the right (indicated by "+" arrow). The two regions are separated by a prominent vertical step at the crevice mouth (at location "0"), better evidenced in Fig. 4. The distinct pyramidal shape of the pits is characteristic of anisotropic (crystallographic orientation-dependent) attack of the faster dissolving (100) and (110) planes, leaving the more stable (111) planes intact. This orientation-dependent dissolution behavior is known to occur in alkaline solutions, such as in KOH and NaOH,[17] it is however usually not observed in media of pH 7.4−7.7. The topography after prolonged immersion has been characterized by 1 mm profilometer linescans across these two regions, one representative example is shown in Fig. 4. Indeed a very prominent vertical step can be seen at the crevice mouth where a maximum depth of ca. 3 μm (corresponding to a dissolution rate of 3.6 nm/h) of Si has almost uniformly corroded away along the whole confined area. Throughout the paper, the corrosion rates in the confined area are calculated based on this maximum uniform dissolution height, Δh_{corr}, measured at the prominent step. Considering the shape of the profile in Fig. 4, and that the most severe damage occurs di-

rectly at the crevice mouth (0 mm), suggests that a galvanic coupling mechanism may be occurring between the electrochemical reactions directly outside in the confined space, balancing the localized corrosion attacks observed inside the crevice. The experiments of the next sections are designed to give more insight into this mechanism. In contrast to the confined/crevice cell immersion conditions, single wafer pieces immersed in bulk HyClone WTF for an equal duration did not show any detectable damage.

Considering 0.01 M PBS, the immersion experiment at 37°C for 35 days showed neither visual nor quantifiably detectable damage, both in the case of the confined/crevice and single wafer samples. Some corrosion was detected however after a much longer immersion time of 157 days in the confined/crevice setup, after which Δh_{corr} was measured to be 170 nm.

HyClone WTF is much more complex in composition than 0.01 M PBS and it is therefore difficult to identify exactly which components are contributing to its harsher influence on Si corrosion. One first hypothesis could be that the protein-containing solution is much more
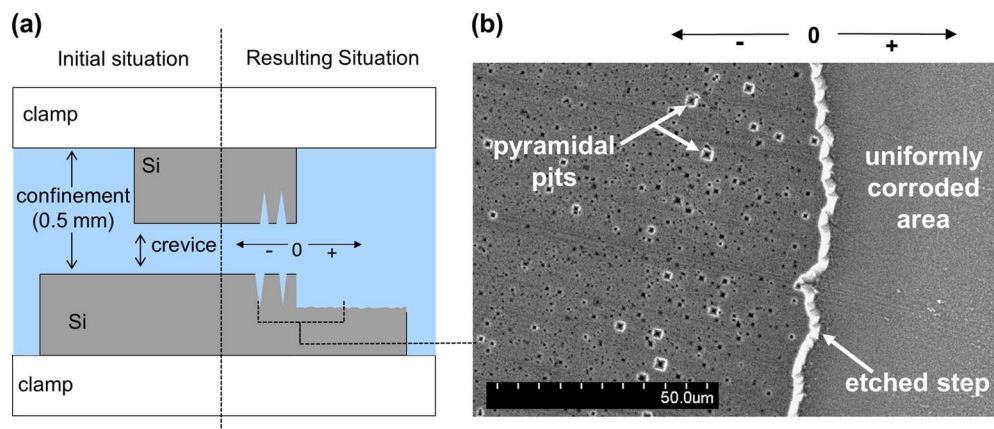

Figure 3. (a) Schematic description (exaggerated for clarification) of the corrosion processes occurring in a Si│Si confined/crevice configuration showing the initial immersion situation, and the resulting situation after 35 days; at the crevice mouth (indicated by "0") a uniformly corroded area occurs to the right in the confinement ("+" arrow), while pits are found to the left inside the crevice ("−" arrow). (b) Resulting SEM image of the bottom Si wafer close to the vicinity of the crevice mouth; unclamped after 35 days in a HyClone WTF containing crevice at 37°C. Pyramidal pits are present in the crevice area, and a distinct step occurs at the crevice mouth where the smaller opposing Si piece was clamped.
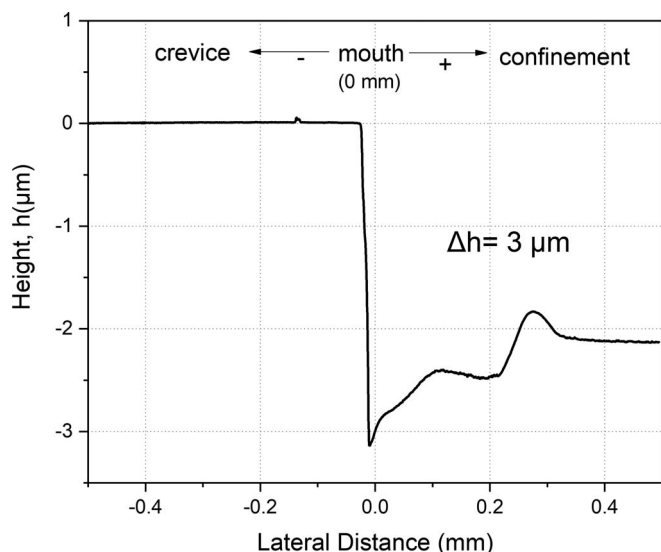
Figure 4. A profilometer topography scan corresponding to Fig. 3b shows a significant corroded depth with a maximum of ca. 3 µm at the mouth (indicated at 0 mm) of the Si │ Si confined/crevice area, after 35 days immersion in HyClone WTF at 37°C.

viscous and hence slows down ionic exchange and diffusion throughout the electrochemical cell.

Accelerated immersion experiments in confined/crevice conditions.—Following the corrosion investigation and processes observed at 37°C, temperature was used as a kinetic acceleration factor to investigate the passive oxide stability threshold and corrosion rates. The resulting corrosion rates of the accelerated Si │ Si confined/crevice immersion experiments at elevated temperatures of 50–90°C are presented in an Arrhenius plot (**ln[corrosion rate] versus 1/T**) in Fig. 5, along with the corrosion rates obtained at 20°C and 37°C. In 0.01 M PBS, the corrosion rates range from 5.4–416.7 nm/h for temperatures between 50–90°C, while in HyClone WTF, measurable corrosion is already initiated at 20°C with corrosion rates of 0.4–13.8 nm/h. The dissolution mechanisms in both solutions yield a linear trend in the Arrhenius plot, suggesting that a single rate-limiting process is occur-
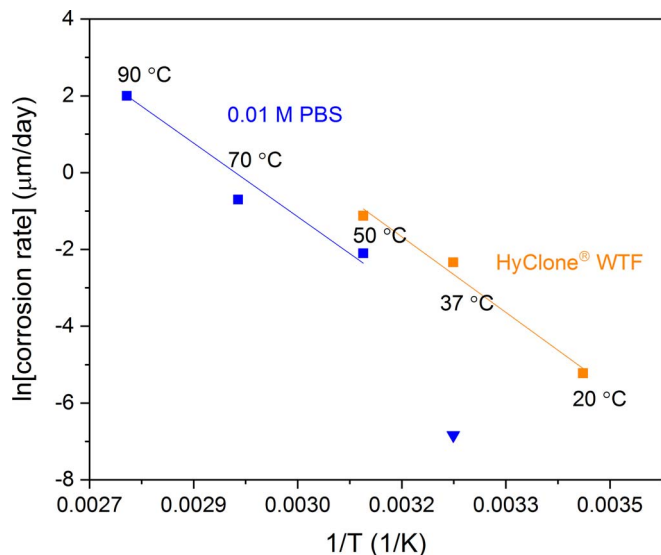

Figure 5. Arrhenius plot demonstrating a linear active Si dissolution mechanism in 0.01 M PBS and HyClone WTF measured in the confined area.
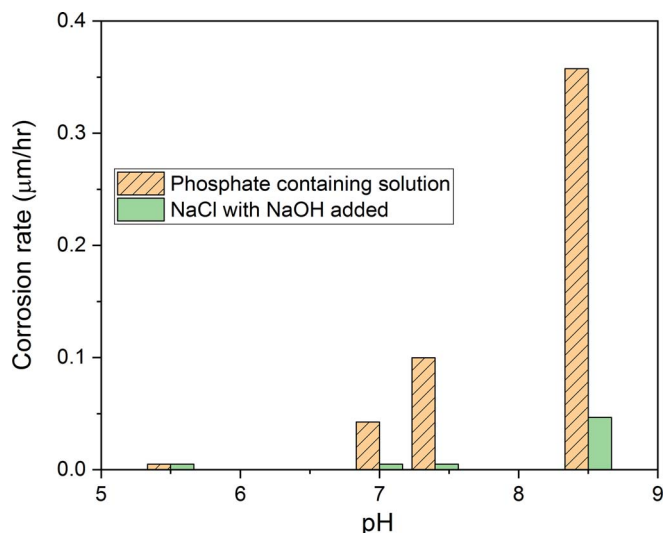

Figure 6. Corrosion rates of Si at the confined area when immersed in NaCl and phosphate-containing crevices (K_2HPO_4, Na_2HPO_4, PBS) at 90°C for 2 h. For NaCl solutions, pH was initially adjusted by NaOH addition.

ring, and that temperature does not alter the dissolution mechanism but only its rate. It has to be mentioned that the corrosion rates are determined assuming immediate corrosion initiation upon immersion and a constant dissolution rate throughout the whole immersion time. This approximation is certainly valid for higher temperature, whereas in the transition temperature range where passivation is still effective, initiation time and mechanisms need to be investigated with more sensitive methods. The immersion experiment performed in 0.01 M PBS at 37°C is a good example supporting the previous statement; the corrosion rate at 37°C was calculated considering a very long immersion duration of 157 days, but active corrosion was likely initiated later, long after the start of immersion. The delayed corrosion initiation explains why the measurement point falls off the Arrhenius trendline. It is a good example of how an in-vitro test performed for a shorter duration may provide misleading predictions of an implant's lifetime, given that the immersion experiment performed for 35 days showed no damage. Therefore, it would be incorrect to guarantee product stability at 37°C, since crevice corrosion can sometimes take many months, or even years, to initiate. When considering the corrosion process for a passivating material like Si, the initiation mechanism is key to understanding its corrosive failure. In the active corrosion domain, the obtained trendlines in Fig. 5 present nearly identical activation energies (E_a), 106 KJ/mol in 0.01 M PBS and 109 KJ/mol in HyClone WTF. The E_a for the dissolution of (100) oriented Si and SiO_2 varies greatly depending on the ionic species present in the solution. In alkaline solutions, the E_a for Si etching can vary between 38–63 KJ/mol and 77–87 KJ/mol for SiO_2, depending on the solution concentration.[18] Van Gelder found activation energies of 110 KJ/mol and 115 KJ/mol, for Si and SiO_2, respectively, etched in phosphorous acid (H_3PO_4).[19] It was suggested that a soluble phosphorous-silicon complex may form, resulting in dissolution of the Si oxide and the substrate. Considering the similar activation energies obtained in this study, the phosphorous species present in PBS and HyClone WTF may contribute to similar phosphorous-silicon complex formation when confined in a small amount of stagnant liquid. To validate this hypothesis, additional experiments were performed to assess the influence that phosphates have on the degradation of Si and are presented in the next section.

Influence of phosphorous species.—While HyClone WTF contains proteins and phosphates but is complex in composition, 0.01 M PBS is a relatively simple solution as it contains only potassium, sodium, chloride, and phosphate compounds. The influence each of these ionic species has on the dissolution of Si and its oxide could be

Table I. Corrosion rates of Si │ Si confined/crevices in different solutions at 90°C. (–) refers to no corrosion detected.

Solution Nr.	Content	Concentration (M)	% $H_2PO_4^-$ / % HPO_4^{2-}	pH	Corrosion rate (nm/h)
1	KH_2PO_4	0.01	99 / 1	5	–
		0.1			
2	NaH_2PO_4	0.01	99 / 1	5	–
		0.1			
3	PBS	0.01	39 / 61	7.4	19
4	K_2HPO_4	0.01	5 / 95	8.5	358
		0.1			1182
5	Na_2HPO_4	0.01	5 / 95	8.5	105
		0.1			830
6	NaCl	0.01	0/0	5.5	–
		0.1			

investigated by performing accelerated Si │ Si confined/crevice immersion experiments in solutions of various salts (Solutions 1–2, and 4–6, in Table I). The experiments were performed with two different solution concentrations (0.01 M and 0.1 M) for 2 h of immersion at 90°C. The measured corrosion rates, determined by means of profilometer linescans (Δh_{corr}) are presented in Table I. Increasing the concentrations of the dibasic phosphate compounds (K_2HPO_4 and Na_2HPO_4) in Solutions 4 and 5 drastically increased the Si corrosion rates. On the other hand, with the monobasic phosphate compounds (KH_2PO_4 and NaH_2PO_4) of Solutions 1 and 2, no corrosion was detected (–) regardless of concentration. The difference lies in the type of phosphate ion that predominates in each solution, which can be determined by a speciation analysis as a function of the pH.[20] The dihydrogen phosphate ion ($H_2PO_4^-$) is weakly acidic and predominates in Solutions 1 and 2, while the hydrogen phosphate ion (HPO_4^{2-}) is weakly alkaline and predominates in Solutions 4 and 5 (see Table I). In 0.01 M PBS, at pH 7.4, the amount of phosphate species are 39% $H_2PO_4^-$ and 61% HPO_4^{2-}. Hence, it appears that the corrosion rate of Si is ultimately enhanced by increasing the alkaline HPO_4^{2-} species in solution. In chloride-containing solution, corrosion was not detected or was much less drastic. Even when chloride-containing solutions were made alkaline by the addition of NaOH, the Si corrosion rates were still much lower than in the phosphate-containing solutions of equal pH, as seen in Fig. 6. These observations indicate that phosphorous-silicon complex formation is a key accelerating factor in the destabilization and corrosion initiation of passivated Si in neutral to slightly alkaline solutions. Si-hydroxide complex formation is then known to be responsible for the dissolution of Si in the more alkaline solutions. Little research has been published on the interaction between phosphate species and Si but given the results presented in this study, a soluble phosphorous-silicon complex as proposed by W. van Gelder,[19] may indeed be the factor controlling oxide film destabilization and active Si dissolution.

Electrochemical characterization of Si passive film stability.—
To investigate the stability of Si oxide and how it relates to corrosion initiation, electrochemical characterization of the potential and current evolution as a function of the immersion conditions (solution, time, and temperature) was performed. Fig. 7 presents the potentiodynamic polarization measurement for Si immersed in bulk 0.01 M PBS and HyClone WTF at 37°C and selected higher temperatures. The polarization measurements obtained for Si immersed in 0.01 M NaCl (pH 5) and NaOH (pH 13) at 37°C are included to demonstrate the passive oxide stability boundary domain; from very protective at pH 5 to active dissolution at pH 13. It can be seen that a kinetic reaction equilibria between oxygen reduction and Si oxidation in the very stable passive surface condition induces nobler (more positive) corrosion potentials (E_{corr}) and lower corrosion current densities (i_{corr}), for Si immersed in NaCl and 0.01 M PBS at 37°C. With increasing pH or temperature, the passive Si-oxides in contact with HyClone WTF and 0.01 M PBS progressively become unstable, as evidenced by a negatively shifting E_{corr} and increasing i_{corr}. Small active-passive transitions in the current curves also start to be observed upon polarization. In NaOH, a very active E_{corr} of ca. -1.2 $V_{Ag/AgCl}$ indicates

complete destabilization of Si-oxide in this media with active dissolution, as expected from the absence of thermodynamically stable phases (Pourbaix diagram[16]). Anodic potentiodynamic polarization however evidences that Si, even in very alkaline pH 13 solution, does not show very high active dissolution current densities. The maximum current density of ca. 10^{-4} A/cm² can be explained by hindered active dissolution related to the formation of poorly soluble Si-complexes (oxi-hydroxides) on the Si surface. Formation of these intermediate products can explain why the Si surface does not remain active and re-passivates when polarizing away from the E_{corr}. This very subtle difference in the surface oxide film stability is demonstrated by the presence of a plateau in the curve upon anodic polarization in pH 13 but with a quite high current density ($> 10^{-5}$ A/cm²), indicating the defective nature of the formed film (referred to as pseudo-passivation).

To better evidence this critical transition from soluble Si-complex formation inducing a decrease in active dissolution, to pseudo-passive oxide formation on the Si surface upon small anodic polarization, potentiostatic polarization experiments were performed in the pH 13 solution around the polarization potentials where the active-passive current transition domain is observed. Indeed, very different current evolution behaviors are recorded when varying the applied potential between -1 $V_{Ag/AgCl}$ and -0.8 $V_{Ag/AgCl}$, as seen by the measurements presented in Fig. 8. The oxide stabilizes with a steady current decrease when the potential is held at -0.8 V, whereas it stays activated (constant higher current) at lower potentials closer to the corrosion potential, E_{corr}. These observations point to a surface oxide which is very sensitive to its chemical environment and is easily stabilized by anodic polarization. For this reason, monitoring the evolution of the
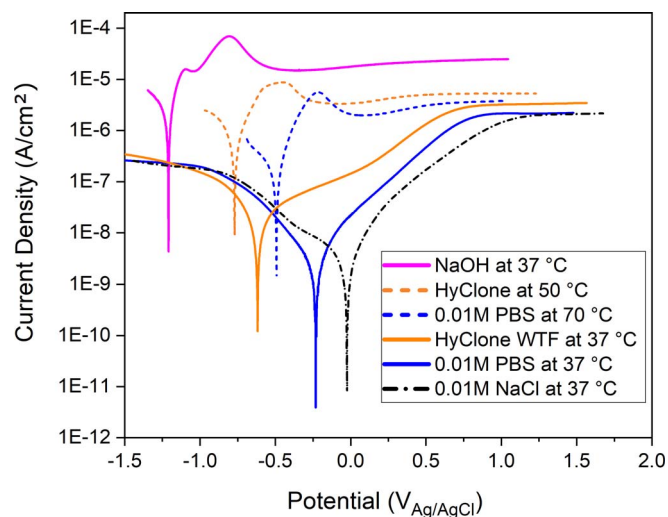

Figure 7. Anodic polarization measurements of Si at different temperatures in bulk solutions: 0.01 M NaCl (pH 5), 0.01 M PBS (pH 7.4), HyClone WTF (pH 7.4–7.7), and NaOH (pH 13).
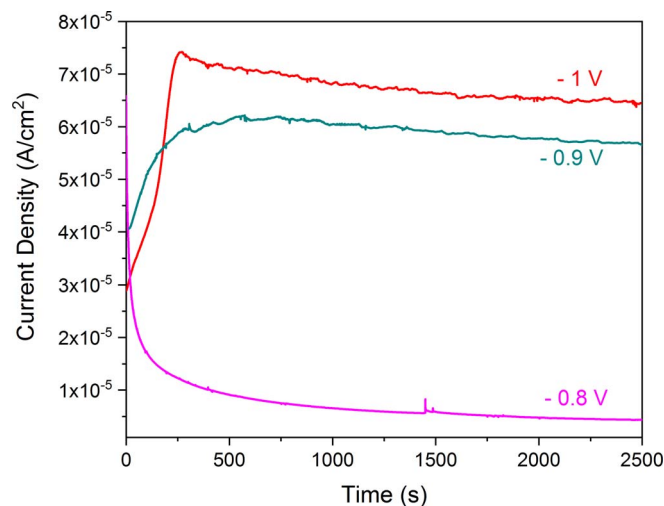
Figure 8. Potentiostatic polarization measurements of Si in bulk NaOH, pH 13, demonstrating the influence of applied potential on the passivation behavior.
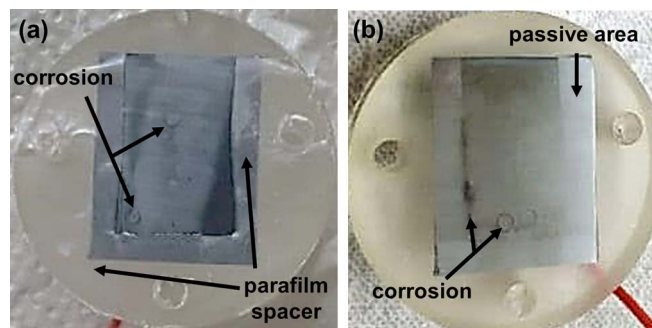

Figure 10. Optical images of Si surfaces after immersion in confined/crevice cells at E$_{corr}$ in: (a) 0.01 M PBS at 50°C for 48 h, then at 70°C for 48 h, and (b) HyClone WTF at 37°C for 48 h, then at 50°C for 48 h.

the active state) to high potentials related to the presence of a stable Si-oxide, as identified by the electrochemical polarizations.

Open circuit potential (OCP) measurements.—OCP measurements were conducted over 48 h on Si working electrodes immersed in bulk solution and in the confined/crevice cell (as described in Fig. 2a). The results are presented in Fig. 9. In the confined/crevice cell, the OCPs measured by the inner and outer RE were nearly identical in the absence of an external cathode, and also related to the very small currents flowing without significant ohmic drops in the system. Hence,
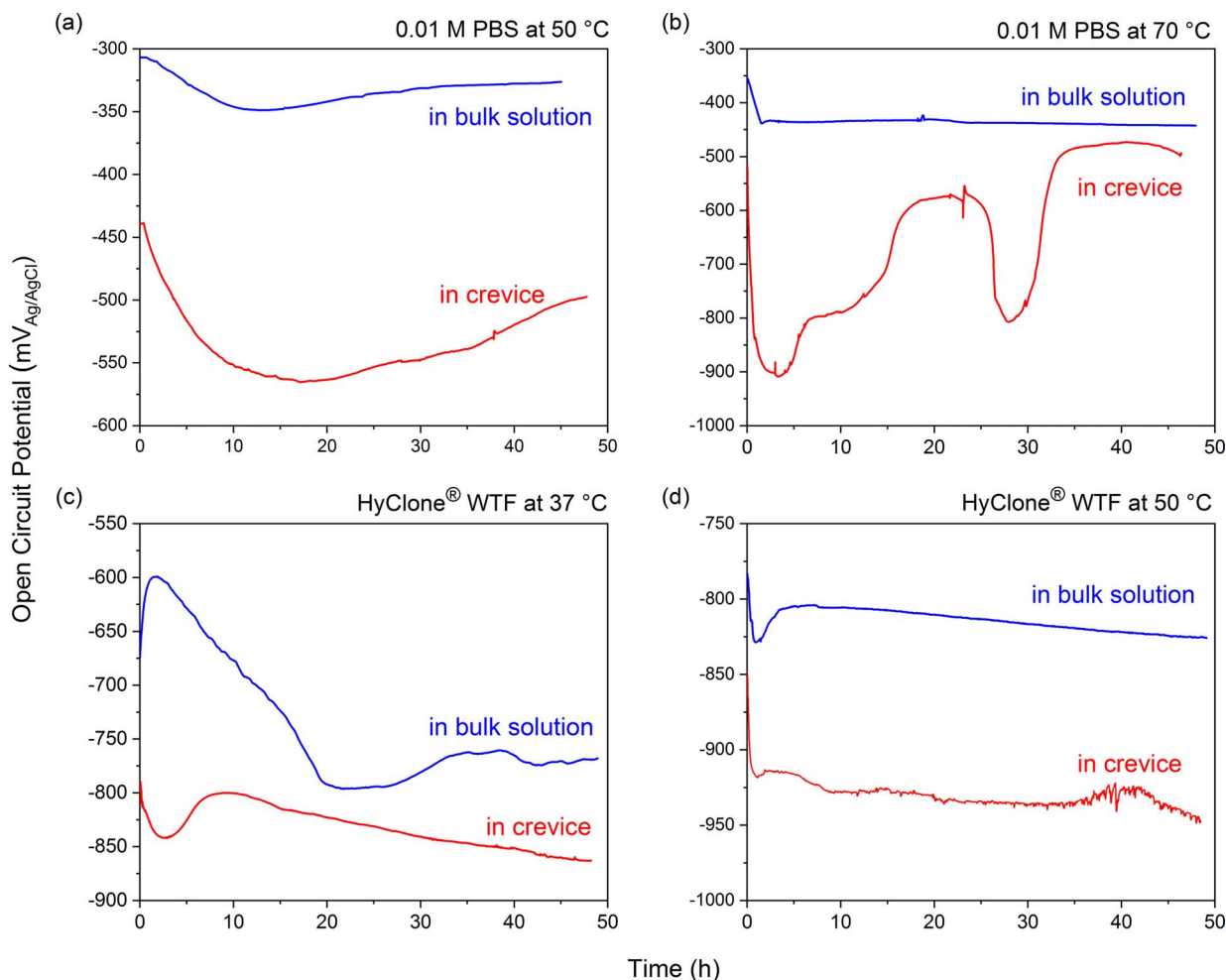
free corrosion potential (OCP) provides a better diagnostic for the surface oxide stability and corrosion initiation susceptibility assessment. Large variations in the measured OCP can be expected depending on the degree of surface stability, from low values (ca. −1.2 V$_{Ag/AgCl}$ in

Figure 9. Open circuit potential (OCP) measurements of Si over 48 h in bulk solution and in the confined/crevice cell configuration: (a) 0.01 M PBS at 50°C, (b) 0.01 M PBS at 70°C, (c) HyClone WTF at 37°C and (d) HyClone WTF at 50°C.
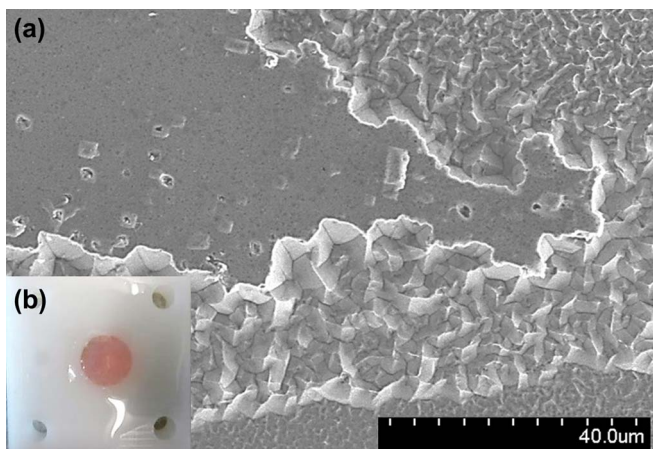
Figure 11. (a) Si after immersion in HyClone WTF (pH 7.4–7.7) for 10 days at 50°C, using the confined configuration from Fig. 2b. Area close to the confinement mouth is shown. (b) Agar infiltrated with phenolthalein turned pink, indicating a pH above 8.5 occurred.

Table II. Influence of Si wafer resistivity on the uniform corrosion rate measured at the confined/crevice border.

Si wafer batch	Resistivity ($\Omega \cdot cm$)	B concentration order (atoms/cm^3)	Corrosion rate (nm/h)
1	0.01	10^{19}	0.04
2	< 0.1	$> 3 \times 10^{17}$	0.05
3	0.2	10^{17}	0.09
4	3–4.2	10^{15}	5.60
5	3–5	10^{15}	2.41
6	5–10	10^{15}	2.71
7	6–7	10^{15}	0.41

as low as ca. -950 mV$_{Ag/AgCl}$ at 50°C. Such low potential values point to a very corrosive system generated by the HyClone WTF, and indeed severe damages were observed when the cell was opened at the end of the experiment, as seen in Fig. 10b.

Influence of Si wafer doping and resistivity on corrosion.— When performing the Si│Si confined/crevice immersion experiments, it was observed that the Si wafer resistivity (dependent on B-doping concentration[21]) directly influenced its corrosion rate. All the experiments presented before were performed with Si wafers having intermediate resistance (Batch 4 in Table II). In order to investigate this dependency, the uniform corrosion rates in the confined/crevice setup geometry were compared for several wafer batches of varying resistivity. The experiments were performed with Si│Si confined/crevices immersed in 0.01 M PBS at 50°C for 20 days. As seen in Table II, the wafers with the lowest resistivity (wafer Batches 1–3), i.e. highest B-doping, showed much lower corrosion rates than those of moderate resistivity (wafer Batches 4–7) with a maximum corrosion rate obtained for Batch 4. This may seem surprising, as an increase in Si conductivity would be expected to increase the corrosion rate, due to the greater availability of electrons for oxidation reactions. A direct correlation between increasing Si conductivity and increasing corrosion rate is indeed obtained when hydrofluoric-based isotropic (very active and uniform dissolution in all orientations) etchants are used; the etching rate increasing at a B concentration above 10^{18} atoms/cm^3.[22] However, the opposite phenomenon, as in our case, has been documented in alkaline anisotropic etchants such as NaOH and KOH. When etching in anisotropic etchants, the Si etching rate greatly reduces in heavily B-doped wafers, commonly referred to as a p+ etch
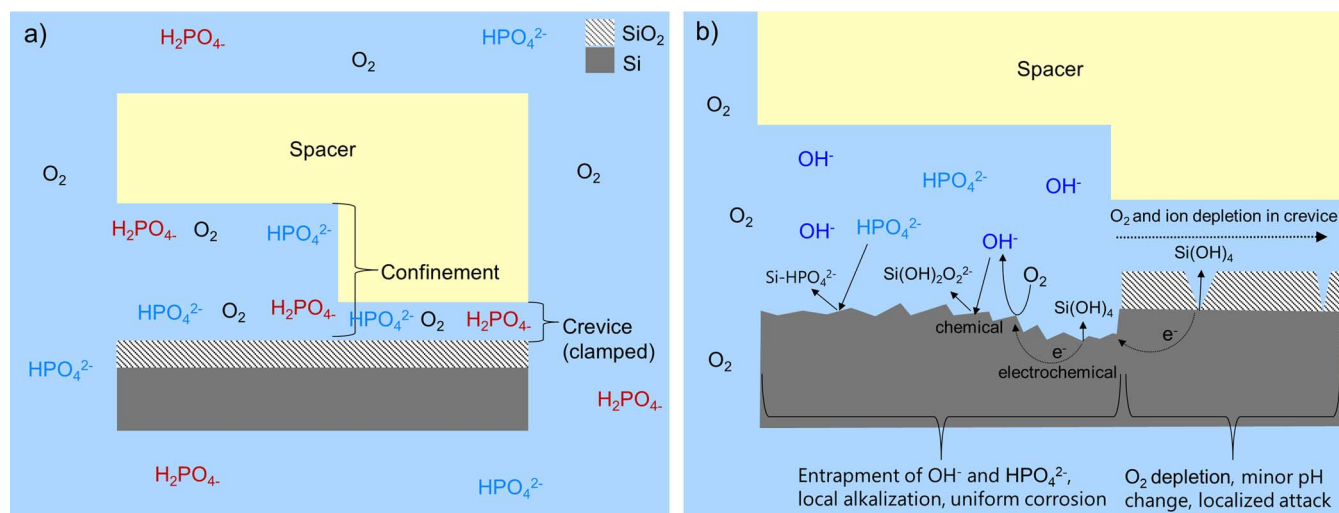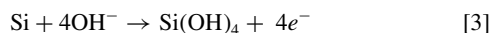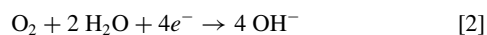
only the OCP evolution at the inner position in the confined area is shown. It can be seen that the OCPs established in the confined area are much more active than the ones measured in bulk solution. This is most evident for samples immersed in 0.01 M PBS at 70°C (Fig. 9b), where the bulk OCP is at a constant noble value for Si of ca. -430 mV$_{Ag/AgCl}$, but the OCP in the confined/crevice cell varies largely between -500 mV$_{Ag/AgCl}$ and -900 mV$_{Ag/AgCl}$. It is important to recall that the Si/SiO$_2$ equilibrium potential is ca. -1000 mV$_{Ag/AgCl}$ at pH 7.4 (in the Si-H$_2$O thermodynamic system). The large potential variation indicates an unstable surface oxide with active corrosion driving the OCP to low values (-900 mV$_{Ag/AgCl}$), and resulting corrosion products (as seen in Fig. 10a) providing some temporary protection of the Si surface, shortly bringing the OCP back up. This OCP fluctuation also shows that the potential decrease cannot be interpreted in terms of oxygen concentration decrease within the confinement, as this would induce a progressive OCP decay for all the experiments. The OCPs measured in HyClone WTF were more active than the ones measured in 0.01 M PBS. Even in bulk HyClone WTF solution, the OCP was fairly active with ca. -600 to -750 mV$_{Ag/AgCl}$ values at 37°C and ca. -800 mV$_{Ag/AgCl}$ at 50°C. The most active OCPs were observed for Si exposed to HyClone WTF in confined/crevice conditions, with values
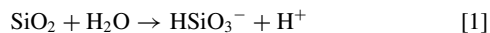

Figure 12. Schematic description of reaction mechanisms showing the influence of a confined/crevice geometry on the dissolution of Si in physiological solutions. a) Initial chemistry at the beginning of the immersion experiment. b) Corrosion mechanisms in the confined/crevice areas at longer immersion times, the areas of interest are enlarged for clarification.

stop.[18,22] Some authors found this etch stop B concentration to be on the order of 10^{19} atoms/cm^3 (ca. 0.01 Ω·cm),[18,23] while others reported it to be on the order of 10^{18} atoms/cm^3 (ca. 0.04 Ω·cm) in dilute KOH solutions.[24] Hence, the findings presented in Table II can be considered consistent with literature. In the confined/crevice geometry, the situation is however slightly different. The higher Si wafer resistivity might explain the trenching (see Fig. 4) observed and the larger corrosion rate measured directly at the border between the crevice and confined area, due to localization of the cathodic reaction (controlling the anodic pitting in the crevice) at the crevice mouth.

pH determination in the confined cell.—In order to confirm that a cathodic-reaction-induced alkaline-type corrosion mechanism could be occurring inside the confined Si area, immersion experiments were performed using the pH-determining device described in Fig. 2b. The device was opened after immersion in HyClone WTF for 10 days at 50°C; the Si surface showed severe anisotropic attack within the area set by the spacer, as seen in Fig. 11a, and the agar infiltrated with phenolthalein was light pink in color, as seen in Fig. 11b. When thymolphthalein was used as the pH indicator, severe attack of the Si surface was also seen, but no color change of the agar was observed. This means that the pH increased and established between 8.5 and 10 within the confined space set by the spacer. The experiments performed in 0.01 M PBS at the same temperature and duration also showed substantial anisotropic attack of the Si, but no color change was observed in the agar. While a surface pH increase on the corroding surface can certainly also occur in PBS, its buffering ability might prevent a measurable pH gradient in the agar.

Discussion of the corrosion mechanism.—Based on the results presented in this study and combining the different aspects of the degradation identified, a simple mechanism explaining the influence of a confined geometry and crevices on the dissolution of Si in physiological simulating solutions is presented in Fig. 12.

Initially, when the confined/crevice cell is immersed (or a defect in DLC coating is exposed to solution), a protective SiO$_2$ film is present on the Si surface. This initial protection can be evidenced by a relatively noble measured E_{corr} value of ca. -400 mV$_{Ag/AgCl}$ in 0.01 M PBS at 37°C (as shown in Fig. 7), corresponding to the kinetic equilibrium between passive Si oxidation and oxygen reduction. The native SiO$_2$ is ca. 1 nm in thickness (as identified by XPS) and in the presence of water can slowly dissociate into soluble ionic species (Equation 1). This may be the initial stage of surface oxide destabilization. In addition, even though SiO$_2$ is in principle an insulator, such a thin oxide can allow electron tunneling from the Si to the oxide surface and provide them for cathodic oxygen reduction (Equation 2), so that the following reactions are possible:

$$SiO_2 + H_2O \rightarrow HSiO_3^- + H^+ \qquad [1]$$

$$O_2 + 2\,H_2O + 4e^- \rightarrow 4\,OH^- \qquad [2]$$

$$Si + 4OH^- \rightarrow Si(OH)_4 + 4e^- \qquad [3]$$

$$Si + H_2O + 2OH^- \rightarrow Si(OH)_2O_2^{2-} + 2H_2 \qquad [4]$$

With time, the O$_2$ in the tight crevice is used up relatively rapidly, while the confined space continues to be supplied by O$_2$. Oxygen reduction therefore predominates in the confined area, resulting in the generation of alkaline OH$^-$ species. With the use of pH indicators, a local pH increase between pH 8.5–10 could be identified in the confined area (as shown in Fig. 11). Cathodic reaction induced local pH increases at a Si-oxide/electrolyte interface could also occur in bulk solution, however these surface pH gradients are short lived, due to better ionic diffusion and equilibration. In a confined geometry, ion diffusion becomes restricted, and accumulation of OH$^-$ can eventually lead to an additional anodic electrochemical (Reaction 3), or chemical (Reaction 4), alkaline-type dissolution mechanism.[25]

Considering purely the chemical equilibria and electrochemical thermodynamic aspects of the Si-H$_2$O system at 25°C (Pourbaix diagram[16]), generation of soluble species and active dissolution in

the confined area would be occurring starting at ca. pH 10. According to the pH range identified experimentally with the pH indicators, pH 10 is not reached in the confined area. The confined electrolyte chemistry might however get close to this pH 10 stability boundary and the surface pH is anyway difficult to assess. Additionally, elevating the temperature narrows the SiO$_2$ thermodynamic stability domain inducing corrosion below pH 10, and the experiments showed clear evidences of slow active dissolution (trenching) especially in the presence of phosphates. Surface activation, identified by a measured OCP decrease down to -850 mV$_{Ag/AgCl}$, occurs already at 37°C in HyClone WTF and is clearly detectable for PBS in confined/crevice conditions from a temperature of 50°C. In addition, when the OCP in the confinement drops to active values of ca. -800 mV$_{Ag/AgCl}$ and -950 mV$_{Ag/AgCl}$ (Fig. 9), cathodic hydrogen reduction can also occur and progressively accelerate corrosion.

Considering the systematic study of the influence of specific anions, phosphates and chlorides (Table I and Fig. 6), it becomes clear that the presence of phosphate is an additional parameter to consider in surface oxide destabilization. For measurements performed at pH 8.5, no uniform corrosion is detected in the confined area in presence of chloride, supporting the fact that the predicted pH 10 oxide stability boundary is valid in absence of the additional phosphate surface interactions. On the other hand, severe corrosion is identified at pH 8.5 in the presence of phosphate species (Table I). The Arrhenius plot in Fig. 5 pointed to an activation energy related to the formation of soluble phosphorous-silicon complexes, as proposed by W. van Gelder.[19]

Lastly, considering in more detail the topography profile of Fig. 4 in relation with the Si resistivity discussion, some assumption can be made about galvanic coupling in the confined/crevice aeration cell geometry. For the middle resistivity domain (Batch 4 Si-wafer: 3–4.2 Ω·cm), a clear trench with enhanced dissolution at the confined/crevice border is continuously observed. For a semiconducting substrate, if a cathodic reaction can take place to initially support the anodic localized dissolution in the crevice, its rate will be higher at the confined/crevice border. The cathodic reaction is related to the observed pH increase, and in the presence of phosphate will increase the corrosion susceptibility also in the confined area. Lowering the resistance of the Si will better distribute the cathodic reaction along the confined surface during the initial stage of localized corrosion in the crevice, and might delay the pH change and detrimental effect in the confined area. This may explain why very low corrosive attack is measured and no trenching is visible in the confined area for the highly conductive wafers. Very high Si resistance on the other hand will hinder galvanic coupling and as a consequence decrease the trenching depth.

One aggravating factor that has not yet been identified is the exact component of the HyClone WTF that has a negative influence on the passive film stability. HyClone WTF already induces increased surface reactivity at 37°C (low OCP, corrosion) in the absence of a confinement/crevice geometry, meaning that its viscosity and hindered ionic diffusion might not be the only detrimental factor contributing to the corrosion mechanism.

Conclusions

An investigation of the corrosion behavior of Si in physiological simulating solutions (0.01 M PBS and HyClone Wear Test Fluid, pH 7.4–7.7) was presented in this study. Long-term and accelerated immersion experiments were developed to investigate the influence of crevices, confined spaces, and bulk solutions on Si stability. Complementary electrochemical measurements were conducted in bulk and confined/crevice configurations to study Si corrosion initiation and oxide stability. The following can be concluded:

• The stability of Si and its naturally grown surface oxide varies drastically between bulk, confined, and crevice immersion conditions.
• In a tight crevice (few microns in thickness), localized corrosion with the formation of pyramidal pits in 0.01 M PBS and HyClone WTF was observed.

- When constricted to a confined (ca. 0.5 mm thick electrolyte)/crevice geometry, Si corroded uniformly up to ca. 3.6 nm/h in HyClone WTF at 37°C, while no measurable damage was observed after exposure in bulk solution.

- Activation (surface oxide destabilization) could be evidenced by in-situ OCP evolution measurements in a confined electrochemical cell geometry; potentials were consistently more active (as low as -950 mV$_{Ag/AgCl}$) compared to the values measured in bulk solution for the simulated physiological solutions considered.

- A higher pH of 8.5–10 was measured in the confined area after immersion in HyClone WTF for several days, indicating that an alkalization process had occurred on the Si surface.

- The corrosion in the confinement was further accelerated by increasing the temperature and a linear Arrhenius trend with activation energies of 106 KJ/mol in 0.01 M PBS, and 109 KJ/mol in HyClone WTF, was observed, corresponding to a phosphorous-silicon interaction mechanism.

- Alkaline phosphate species contributed to accelerating the Si corrosion initiation and dissolution rates, whereas chlorides seemed to have little influence on the Si corrosion susceptibility.

- The overall corrosion mechanism is initiated by galvanic coupling, as observed by the separation of pitting in the crevice and trenching at the border with the confined area, pH increase and phosphorous-silicon complexation.

Overall, when determining the stability of biomedical implantable components, this study illustrates the importance of considering geometrical aspects for in-vitro testing procedures, aspects which can be inherent of the implant design or generated by contact with tissue in the in-vivo environment. These findings can be used to provide better predictions of the lifetime of implantable Si components and Si-based interlayers, as well the presented methodologies can be applied to any other material of interest.

Acknowledgments

ORCID

Emilija Ilic https://orcid.org/0000-0002-0220-1258

References

1. D. J. Edell, *Neuroprosthetics: Theory and Practice*, K. H. Horch and G. S. Dhillon, Editors, 2nd ed., p. 517, Utah (2014).
2. E. Fernandez and R. Normann, *Introduction to Visual Prostheses*, H. Kolb, E. Fernandez, and R. Nelson, Editors, p. 11, Salt Lake City (2016).
3. M. Azzi, P. Amirault, M. Paquette, J. E. Klemberg-Sapieha, and L. Martinu, *Surf. Coatings Technol.*, **204**, 3986 (2010).
4. R. Butter, M. Allen, L. Chandra, A. H. Lettington, and N. Rushton, *Diam. Relat. Mater.*, **4**, 857 (1995).
5. A. Vanhoestenberghe and N. Donaldson, *J. Neural Eng.*, **10**, 13 (2013).
6. G. Taeger, L. E. Podleska, B. Schmidt, M. Ziegler, and D. Nast-Kolb, *Materwiss. Werksttech.*, **34**, 1094 (2003).
7. R. Hauert, C. V. Falub, G. Thorwarth, K. Thorwarth, Ch. Affolter, M. Stiefel, L. E. Podleska, and G. Taeger, *Acta Biomater.*, **8**, 3170 (2012).
8. R. Hauert, K. Thorwarth, and G. Thorwarth, *Surf. Coatings Technol.*, **233**, 119 (2013).
9. R. Hauert, G. Thorwarth, U. Müller, M. Stiefel, C. V. Falub, K. Thorwarth, and T. J. Joyce, *Diam. Relat. Mater.*, **25**, 34 (2012).
10. J. C. Barrese, J. Aceros, J. P. Donoghue, R. Island, and R. Island, *J Neural Eng.*, **13**, 27 (2016).
11. H. Hämmerle, K. Kobuch, K. Kohler, W. Nisch, H. Sachs, and M. Stelzle, *Biomaterials*, **23**, 797 (2002).
12. D. J. Edell, D. Drive, and E. Suite, in *Materials Research Society Symposium Proceedings*, vol. **773**, p. N1.9.1 (2013).
13. J. Morales, J. Souriau, and G. Simon, *ECS Trans.*, **69**, 9 (2015).
14. J. M. Maloney, S. A. Lipka, and S. P. Baldwin, in *Materials Research Society Symposium Proceedings*, vol. **872**, p. J14.3.1 (2005).
15. M. Fröhlich, M. Birkholz, K. E. Ehwald, P. Kulse, O. Fursenko, and J. Katzer, in *IOP Conference Series: Materials Science and Engineering*, vol. **41**, p. 012022 (2012).
16. J. Van Muylder, J. Besson, W. Kunz, and M. Pourbaix, in *Atlas of Electrochemical Equilibria in Aqueous Solutions*, p. 459, NACE, Houston (1974).
17. O. Powell and H. B. Harrison, *J. Micromechanics Microengineering*, **11**, 217 (2001).
18. H. Seidel, L. Csepregi, A. Heuberger, and H. Baumgärtel, *J. Electrochem. Soc.*, **137**, 3612 (1990).
19. W. van Gelder and V. E. Hauser, *J. Electrochem. Soc.*, **114**, 869 (1967).
20. P. Hinsinger, *Plant Soil*, **137**, 173 (2001).
21. W. R. Thurber, R. L. Mattis, Y. M. Liu, and J. J. Filliben, *Semiconductor measurement technology: The relationship between resistivity and dopant density for phosphorus and boron doped silicon.*, p. 42, Washington, (1981).
22. C. A. Zorman and M. Mehregany, in *The MEMS handbook. MEMS: Design and fabrication*, M. Gad-el-Hak, Editor, p. 1, Taylor & Francis Group (2006).
23. A. Bogh, *J. Electrochem. Soc.*, **118**, 401 (1971).
24. J. B. Price, H. R. Huff, and R. R. Burgess, in *Semiconductor Silicon*, p. 339, *The Electrochemical Society Softbound Symposium*, Princeton, N.J. (1973).
25. X. G. Zhang, *Electrochemistry of silicon and its oxide*, Kluwer Academic/Plenum Publishers, New York (2001).